

Quadratically Transformed Luminance Chrominance Spaces

Giulio Biondi(✉), Antonio Boccuto, and Ivan Gerace

Department of Mathematics and Computer Science, University of Perugia, Perugia, Italy
{giulio.biondi,antonio.boccuto,ivan.gerace}@unipg.it

Abstract. Several color spaces defined in the literature are obtained from the RGB space through non-linear transforms, potentially limiting their applicability in a regularization context. Therefore, in this paper, we introduce three new color spaces, QTLC-r_*^2, QTLC-g_*^2, and QTLC-r_*g_*, and the corresponding quadratic mappings from the RGB space. To test their uniformity, we use them to consider the image defading problem through a novel two-step technique: first, we define a fast heuristic to restore the natural color saturation; then, we propose a regularization technique to deblur the image. We experimentally observe that presumably thanks to its higher uniformity, the QTLC-r_*g_* space produces natural-looking images in the reconstruction and should be preferred to the QTLC-r_*^2 and QTLC-g_*^2 spaces.

Keywords: uniform color space · defading problem · deblurring · regularization technique

1 Introduction

A color space is said to be *uniform* if the adjacent colors in it are similar to the human eye [9,11]. The classical color spaces, as RGB (*Red-Green-Blue*) and CMYK (*Cyan-Magenta-Yellow-Black*), are not uniform. The uniform color spaces, in general, are defined as employing luminance and chrominance components, since these two components have different properties. The most known classical space constructed in this way is the CIE $L^*a^*b^*$ space. Unfortunately, in general, the transform from *RGB* to CIE $L^*a^*b^*$ is not polynomial and not easily manageable. The aim of this article is to study some new color spaces which are defined using luminance and chrominance, using a quadratic transform to compute the coordinates of color from the RGB space to them. In particular we define three different color spaces, which we call QTLC-r_*^2 (*Quadratically Transformed Luminance Chrominance-*r_*^2), QTLC-g_*^2, and QTLC-$r_*\,g_*$. The choice of quadratic transforms and rational numerical coefficients for the proposed mappings aims to define simple models yet deliver performance comparable to existing state-of-the-art methods, to enhance their applicability to downstream tasks, e.g., image demosaicing (see, e.g., [3,13]) and optical flow (see, e.g., [12,16]). In

© The Author(s), under exclusive license to Springer Nature Switzerland AG 2023
O. Gervasi et al. (Eds.): ICCSA 2023 Workshops, LNCS 14108, pp. 676–693, 2023.
https://doi.org/10.1007/978-3-031-37117-2_45

this work, to test such spaces, we deal with the defading image problem [1]. The problem of faded images refers to the loss of quality and detail in an image over time due to environmental factors such as light exposure, temperature, and humidity. This results in the colors becoming less vibrant, the contrast is reduced, and the details becoming less sharp. Faded images can also be caused by the deterioration of the physical materials used to store the image, such as film or paper. This can be a significant issue for individuals, archives, and museums that aim to preserve historical images and visual artifacts. To address this problem, several methods are available for restoring faded images, including digital restoration techniques (see, e.g., [1,15,19,21]) and chemical treatments for physical media. However, there are several reasons why digital restoration may be preferred over physical restoration for faded images.

- Speed and convenience: Digital restoration can be performed quickly and easily using specialized software and hardware. On the other hand, physical restoration can be time-consuming and labor-intensive.
- Non-invasivity: Digital restoration requires no physical intervention with the original image. On the other hand, physical restoration can sometimes further damage the image.
- Flexibility: Digital restoration allows for easy adjustments and changes to the image during restoration. Physical restoration, once completed, cannot be easily altered.
- Reproduction: Digital restoration allows for the creation of multiple copies of the restored image, which can be distributed and shared more easily than physical copies.
- Preservation: Digital restoration enables the preservation of the restored image in a digital format, which can be easily backed up and protected against future degradation. Physical restoration is subject to ongoing degradation and requires ongoing preservation efforts.
- Accessibility: Digital restoration makes the restored image more widely accessible to a larger audience, including people with disabilities and those in remote locations. Physical restoration is typically limited to those who can physically access the location where the image is housed.

The *defading image problem* consists in estimating the ideal source image, given a faded image. To solve this problem, we proceed in two phases. In the former, we define a simple heuristic to recover the correct color saturation of the image. However, some unsupervised techniques are described in the literature (see, e.g., [6,20]). Concerning the latter, we propose a novel two-step approach. In the first we reconstruct the luminance component and use a regularization technique, through which the solution is defined as the minimizer of a suitable energy function. In such a function, some constraints are included, which impose that the second–order finite differences of luminance are small enough, and allow the existence of discontinuities of the values of luminance. Indeed, we can assume that luminance is a piecewise linear function [7]; moreover, to further increase the quality of the reconstruction, we inhibit the existence of parallel adjacent discontinuities (see, e.g., [2,4,5]). To minimize the energy function, we use a GNC

(*Graduate Non-Convexity*) technique (see, e.g., [2,5,7,10,14,17,18,22,23]). In the second step, we assume that chrominance is a piecewise constant function and that the discontinuities present in such a function correspond to those estimated for the luminance. So, the regularized solution is defined as a minimizer of a different energy function. Since such a function is convex, the minimization can be performed by a SOR (*Successive Over Relaxation*) algorithm. The experimental results show how the QTLC-r_*g_* space gives the most natural results in reconstructing faded images.

The article is structured as follows. In Sect. 2 we introduce three new color spaces, in Sect. 3 we deal with the defading problem, and in Sect. 4 we present our experimental results.

2 New Luminance-Chrominance Spaces

In this section, we introduce some new spaces defined using luminance and chrominance, obtained by a transform from the RGB space. In particular, we consider Adobe RGB, where each color is encoded as a triple $(r, g, b) \in [0, 1]^3$. Let us first consider the following coordinate change

$$\begin{cases} l = \dfrac{1}{4}\, r + \dfrac{1}{2}\, g + \dfrac{1}{4}\, b, \\ r_* = \dfrac{r - l}{l}, \\ g_* = \dfrac{g - l}{l}. \end{cases}$$

We determine the value of the luminance coordinate l as a linear combination of the terms r, g, b, so that the sum of the involved coefficients is equal to 1 and, to describe a realistic model, the coefficient corresponding to the green color is the largest one since the human eye perceives green better than the other colors. The pair of coordinates (r_*, g_*) represents the chrominance of the color; note that, in this color space, every gray corresponds to the origin $(0, 0)$.

Now we find three quadratic transforms that map the subspace (r_*, g_*) into the subspace (α, β); in particular, we focus on mapping the Aqua Green, Magenta, Gray, and Blue colors into $(\alpha, \beta) = (-1, 0)$, $(\alpha, \beta) = (1, 0)$, $(\alpha, \beta) = (0, 0)$, and $(\alpha, \beta) = (0, -1)$, respectively (see Table 1), so that complementary colors are symmetrical with respect to the origin. In Fig. 1 the desired color mapping is illustrated.

We consider the following transforms:

$$\begin{cases} \alpha = \dfrac{19}{40} r_* - \dfrac{5}{8} g_* - \dfrac{3}{20}\, r_*^2 \\ \beta = \dfrac{3}{8} r_* + \dfrac{5}{8} g_*, \end{cases} \tag{1}$$

Table 1. Color coordinates in the spaces (r, g, b), $(l, \overline{r}, \overline{g})$, (l, r_*, g_*), (l, α, β).

	r	g	b	l	r_*	g_*	α	β
Gray	k	k	k	k	0	0	0	0
Magenta	1	0	1/2	3/8	5/3	-1	1	0
Aqua Green	0	1	1/2	5/8	-1	3/5	-1	0
Blue	0	0	1	1/4	-1	-1	0	-1

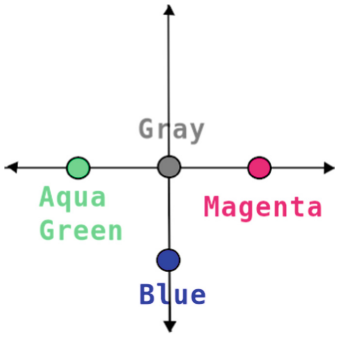

Fig. 1. Colors mapping in the proposed spaces

$$\begin{cases} \alpha = \dfrac{3}{8} r_* - \dfrac{19}{24} g_* - \dfrac{5}{12} g_*^2 \\ \beta = \dfrac{3}{8} r_* + \dfrac{5}{8} g_*, \end{cases} \tag{2}$$

$$\begin{cases} \alpha = \dfrac{5}{8} r_* - \dfrac{3}{8} g_* + \dfrac{1}{4} r_* g_* \\ \beta = \dfrac{3}{8} r_* + \dfrac{5}{8} g_*, \end{cases} \tag{3}$$

Note that β reduces to a linear function of r_* and g_*; furthermore, a quadratic term is necessary for the transforms to be well-defined.

The spaces obtained by the transform in (Eq. 1), (Eq. 2), and (Eq. 3) are called *Quadratically Transformed Luminance Chrominance* r_*^2 (QTLC-r_*^2), *Quadratically Transformed Luminance Chrominance* g_*^2 (QTLC-g_*^2), and *Quadratically Transformed Luminance Chrominance* $r_* g_*$ (QTLC-$r_* g_*$), respectively. In Fig. 2, in (a), (b), and (c), the sections of the QTLC-r_*^2, QTLC-g_*^2, and QTLC-$r_* g_*$ spaces are represented for $l = 180$, respectively. Figure 2 (d) shows the section of the CIE $L^*a^*b^*$ space for $l = 100$; in the CIE $L^*a^*b^*$ space $l \in [0, 100]$ and, for the chrominance components, $a^* \in [-500, 500]$, and $b^* \in [-200, 200]$. In (a), in correspondence with the orange color, a sharp gradient can be observed; in (b), in the lower right section, there is a compenetration

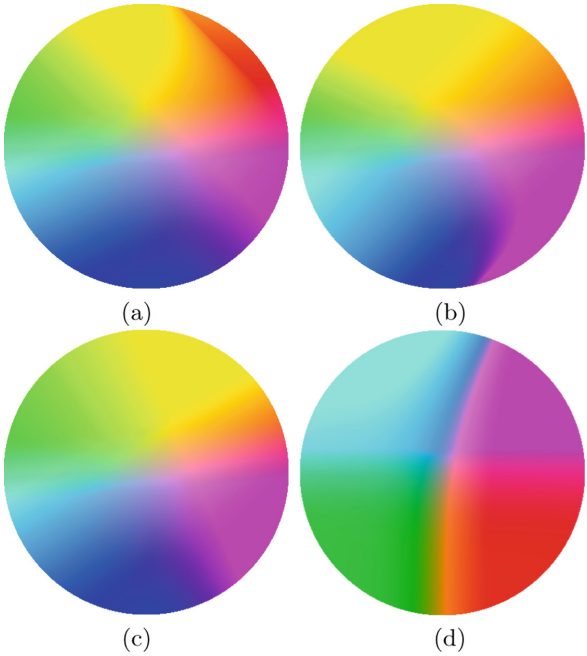

Fig. 2. Sections of the spaces QTLC-r_*^2 (a), QTLC-g_*^2 (b), QTLC-$r_*\, g_*$ (c) for $l = 180$, and in the CIE $L^*a^*b^*$ space for $l = 100$ (d).

between the blue and the magenta clues; the plot of (c), instead, shows a closer behavior to that of a uniform space. From visual inspections on various values of l, the behavior appears to be consistent. In Fig. 3 the luminance component in the QTLC-r_*^2, QTLC-g_*^2, and QTLC-$r_*\, g_*$ spaces (b) and in the CIE $L^*a^*b^*$ space (c) are shown next to the source image (a); the chrominance components, instead, are visualized in Fig. 4. Each row shows, from left to right, the α, β, and total chrominance (α, β) for, respectively, the QTLC-r_*^2, QTLC-g_*^2, and QTLC-$r_*\, g_*$ spaces; in the final row, the a^*, b^* and (a^*, b^*) components in the CIE $L^*a^*b^*$ space. For all the QTLC spaces, the representations do not show appreciable differences. Moreover, regardless of the space, luminance is associated with image details, while chrominance is used for color distribution. Note that these two properties can be modeled as functions whose behavior is close to be piecewise linear and piecewise constant, respectively.

3 The Defading Image Problem

We now show how the spaces introduced in the previous section can be used to solve the defading image problem. Old images can be faded because of light damage, air exposure, mold and fungi, improper storage, or water damage. Due



(a) (b) (c)

Fig. 3. (a) The source image; (b) the luminance component in the QTLC-r_*^2, QTLC-g_*^2, and QTLC-$r_*\, g_*$ spaces; (c) the luminance component in the CIE $L^*a^*b^*$ space.

to these effects, we get both a variation of saturation of the involved colors and a blur on the image.

Our proposed method is divided into two phases. The former emphasizes the involved colors by intensifying the contrasts and is necessary to get the correct saturation in the estimated ideal image. In the latter, the analyzed image is deblurred.

3.1 Analysis of the Contrast

For testing, we employ a simple heuristic to intensify the contrast of a faded image. First, we analyze the luminance value. A faded image of size $n \times m$ can be expressed as $f = (\mathbf{l}, \boldsymbol{\alpha}, \boldsymbol{\beta}) \in \mathbb{R}^{n \times m \times 3}$, where $(\mathbf{l}, \boldsymbol{\alpha}, \boldsymbol{\beta})$ are, respectively, the vectors in lexicographic form of the luminance, α-chrominance and β-chrominance. It is necessary to determine empirically a value l_0 of the luminance, which we want to be constant. So, the luminance value at every pixel $(i, j) \in \{1, \ldots, n\}^2$ is modified according to the following algorithmic law:

$$l(i,j) := (c_l(l(i,j) - l_0) + l_0)^{(+)},$$

where $c_l > 0$ is the contrast parameter, which expresses the sharpness of the contrast, and $\tau^{(+)} = \max\{\tau, 0\}$. The choice of c_l is made empirically, according to the characteristics of the image.

Concerning the value of chrominance, we proceed analogously. In particular, we consider the positive and the negative values of $\boldsymbol{\alpha}$ and $\boldsymbol{\beta}$ separately. Namely, we fix four different saturation values, which we want to be constant, which we call α_0^+, α_0^-, β_0^+, β_0^-, which correspond to the values of Magenta, Aqua Green, Yellow and Blue, respectively. Note that α_0^+ and β_0^+ are positive, while α_0^- and β_0^- are negative. Moreover, we fix the contrast parameter for the four involved colors, which we call c_α^+, c_α^-, c_β^+, c_β^-. For every $(i, j) \in \{1, \ldots, n\} \times \{1, \ldots, m\}$

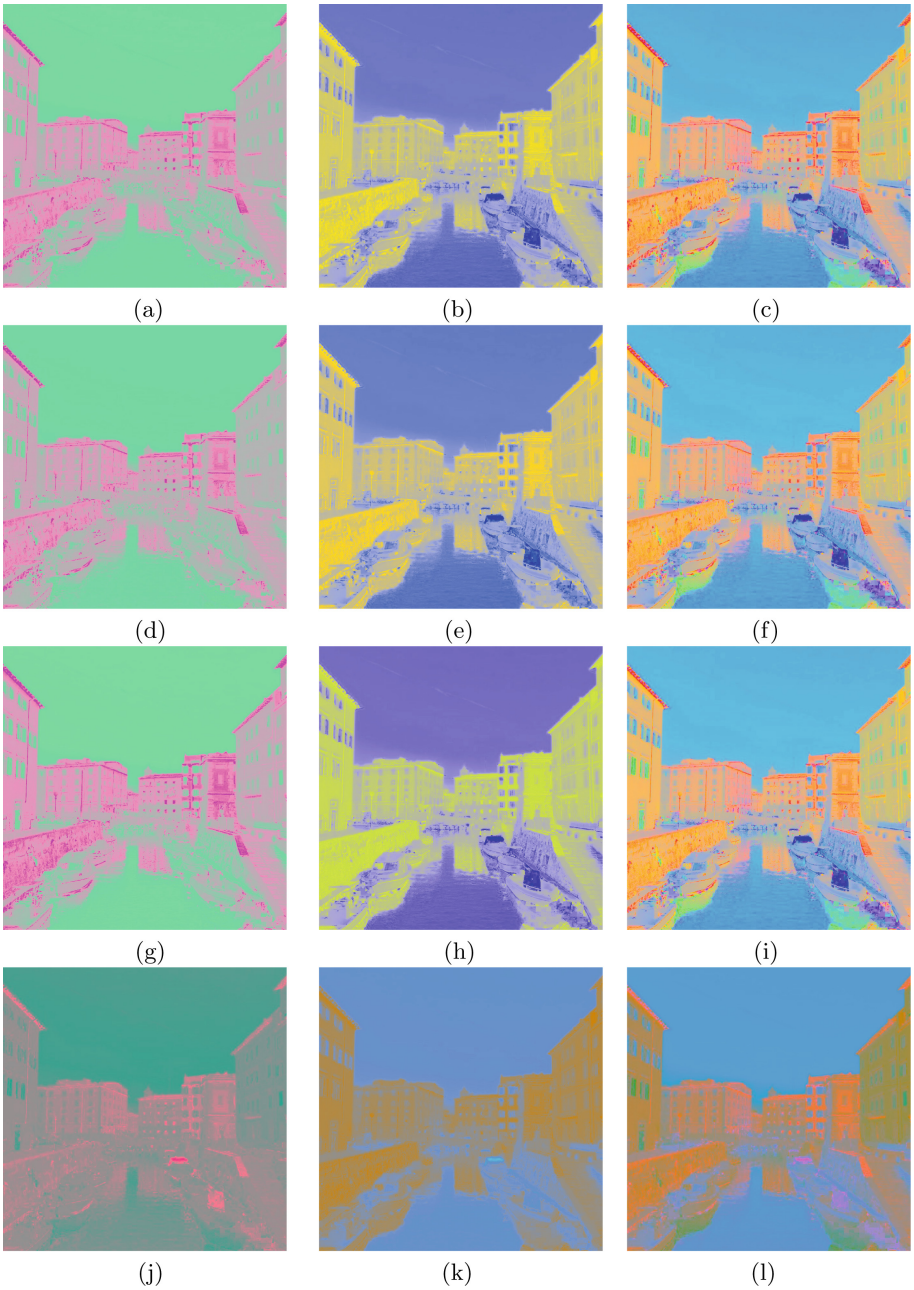

Fig. 4. The α (a), β (b) and total (c) chrominance associated with the QTLC-r_*^2 space; the α (d), β (e) and total (α, β) (f) chrominance related to the QTLC-g_*^2 space; the α (g), β (h) and total (i) chrominance corresponding to the QTLC-$r_*\, g_*$ space; the a^* (j), b^* (k) and (a^*, b^*) (l) components in the CIE $L^*a^*b^*$ space. (Color figure online)

we apply

$$\alpha(i,j) = \begin{cases} (c_\alpha^+(\alpha(i,j) - l_\alpha^+) + l_\alpha^+)^{(+)} \text{ if } \alpha(i,j) \geq 0, \\ (c_\alpha^-(\alpha(i,j) - l_\alpha^-) + l_\alpha^-)^{(-)} \text{ if } \alpha(i,j) < 0, \end{cases}$$

$$\beta(i,j) = \begin{cases} (c_\beta^+(\beta(i,j) - l_\beta^+) + l_\beta^+)^{(+)} \text{ if } \beta(i,j) \geq 0, \\ (c_\beta^-(\beta(i,j) - l_\beta^-) + l_\beta^-)^{(-)} \text{ if } \beta(i,j) < 0, \end{cases}$$

where $\tau^{(-)} = \min\{\tau, 0\}$.

3.2 The Deblurring Technique

In our approach, luminance and chrominance are deblurred separately. Indeed, as we can see in Fig. 4 (b), luminance corresponds to the analyzed color image transformed into a grayscale image, while chrominance corresponds to an image with almost constant color stains. Such a difference requires the two components to be treated separately; for this reason, we model luminance using a piecewise linear function, and chrominance of a piecewise constant function.

Luminance Deblurring. The problem of luminance deblurring is similar to that of reconstructing the original grayscale image from a grayscale image blurred and/or corrupted by noise. The direct problem is stated as follows:

$$\mathbf{l} = A\widetilde{\mathbf{l}} + \mathbf{n_l},$$

where the vectors $\mathbf{l}, \widetilde{\mathbf{l}}$, of dimension $n\,m$, are the observed luminance and the ideal one in the lexicographic order, respectively. The vector $\mathbf{n_l}$, of dimension $n\,m$, is the additive noise on the luminance, which we assume to be white, Gaussian, with zero mean and a known variance σ^2. The $(n\,m) \times (n\,m)$-matrix A is a linear operator, which represents the blur acting on the luminance. Each pixel of the blur luminance is assumed to be obtained by a weighted average of its neighbors. Given a positive matrix $M \in \mathbb{R}^{(2h+1)\times(2h+1)}$, called *blur mask,* the entries of matrix A can be defined by:

$$a_{(i,j),(i+w,j+v)} = \begin{cases} \dfrac{m_{h+1+w,h+1+v}}{\nu_{i,j}}, \text{ if } |w|, |v| \leq h, \\ 0, \qquad\qquad \text{otherwise,} \end{cases}$$

where $\nu_{i,j} = \sum_{i=\xi_1}^{\xi_2} \sum_{j=\xi_3}^{\xi_4} m_{i,j}$, $\xi_1 = \max\{1, 2+h-i\}$, $\xi_2 = \min\{2h+1, n-i+h+1\}$, $\xi_3 = \max\{1, 2+h-j\}$, and $\xi_4 = \min\{2h+1, n-j+h+1\}$.

In this work, we reduce the problem to a luminance restoration problem, which consists in finding an estimation $\widetilde{\mathbf{l}}$ of the unknown original luminance,

given the blurred luminance $\mathbf{l}$, the matrix A and the variance of the noise σ^2; for the sake of simplicity, A is determined empirically. This is an ill-posed inverse problem in the sense of Hadamard (see, e.g., [8]).

To solve ill-posed problems, a *regularization technique* is used in order to find a unique solution, stable concerning the noise. To improve the quality of the results, some binary elements called *line variables*, can be considered (see, e.g., [5]). These elements consider the discontinuities present in the luminance $\widetilde{\mathbf{l}}$ the ideal luminances have discontinuities in correspondence with the edges of different objects. A *clique* c of order 1 (resp., 2) is a subset of points of a square grid on which the first (resp., second) order finite difference is defined. We denote by the symbol C_1 (resp., C_2) the set of all cliques of order 1 (resp., 2), namely $C_1 = \{c = \{(i,j),(h,l)\} : i = h, j = l+1 \text{ or } i = h+1, j = l\}$ (resp., $C_2 = \{c = \{(i,j),(h,l),(r,q)\} : i = h = r, j = l+1 = q+2 \text{ or } i = h+1 = r+2, j = l = q\}$). We denote the first (resp., second) order finite difference operator of the vector $\widetilde{\mathbf{l}}$ associated with the clique c by $D_c^k\widetilde{\mathbf{l}}$, $k = 1, 2$, that is, if $c = \{(i,j),(h,l)\} \in C_1$, then $D_c^1\mathbf{x} = x_{i,j} - x_{h,l}$, (resp., if $c = \{(i,j),(h,l),(r,q)\} \in C_2$, then $D_c^2\mathbf{x} = x_{i,j} - 2x_{h,l} + x_{r,q}$). Note that the second–order differences are used for the luminance restoration problem, while the first order differences will be considered in the next paragraph for the chrominance deblurring.

Now, let us introduce the auxiliary variables associated with the discontinuities of the luminance $\widetilde{\mathbf{l}}$. A good estimation of the discontinuities is crucial to restoring luminance quality. Such variables have the role of eliminating the regularity constraint, where discontinuities should appear. To every clique c we associate a weight $w_c \in \{0, 1\}$, called *line variable*; in particular, a value of 1 corresponds to a discontinuity in luminance in c. The vector $\mathbf{w}$ is the set of all line variables w_c. Thus, the original luminance is considered as a pair $(\widetilde{\mathbf{l}}, \mathbf{w})$, where $\widetilde{\mathbf{l}}$ is the matrix of the luminance levels of pixels, and $\mathbf{w}$ is the vector of the set of all components w_c, $c \in C_2$. Let us introduce the concept of *adjacent clique of order* 2, which is used to define the non-parallelism constraint. Given a vertical clique $c = \{(i,j),(i+1,j),(i+2,j)\}$, $i = 3, \ldots, M-2$, $j = 1, \ldots, N$, we define its preceding clique $c-1$ as follows:

$$c - 1 = \{(i-2,j),(i-1,j),\ldots,(i,j)\}.$$

If c is a horizontal clique, $c = \{(i,j),(i,j+1),(i,j+2)\}$, $i = 1, \ldots, M$, $j = 3, \ldots, N-2$, then its preceding clique $c-1$ is defined by setting

$$c - 1 = \{(i,j-2),(i,j-1),(i,j)\}.$$

We use the convention that if $c-1$ does not exist, then $w_{c-1} = 0$.

A regularized solution to the restoration problem is achieved as the minimum of the *primal energy function*, given by

$$E(\widetilde{\mathbf{l}}, \mathbf{w}) = \|A\widetilde{\mathbf{l}} - \mathbf{l}\|^2 + \sum_{c \in C_2} \left[\lambda^2 (D_c^2\widetilde{\mathbf{l}})^2 (1 - w_c) + \theta w_c\right] + \sum_{c \in C_2} \varepsilon\, w_c\, w_{c-1}. \quad (4)$$

The first term of (Eq. 4) measures the faithfulness of the solution to the data. The second one is a regularization term related to a smoothness condition on $\widetilde{\mathbf{l}}$. The *regularization parameter* λ^2 allows us to establish an appropriate degree of smoothness in the solution. The positive parameter θ is used to avoid having too many discontinuities in the restored luminance. The last term, $\varepsilon \geq 0$, is added to the energy function to make parallel close discontinuities in the restored luminance unlikely to appear. The importance of ε is apparent in Fig. 5; the image in (b) is reconstructed from the blurred image in (a) by setting $\varepsilon = 0$, i.e., not using it, while the image in (d) by setting ε to an appropriate strictly positive value. Although the reconstructions of Fig. 5 (b) and (d) appear similar to the human eye, the underlying quality for the latter is higher, as visible in the corresponding line process plots (c) and (e).

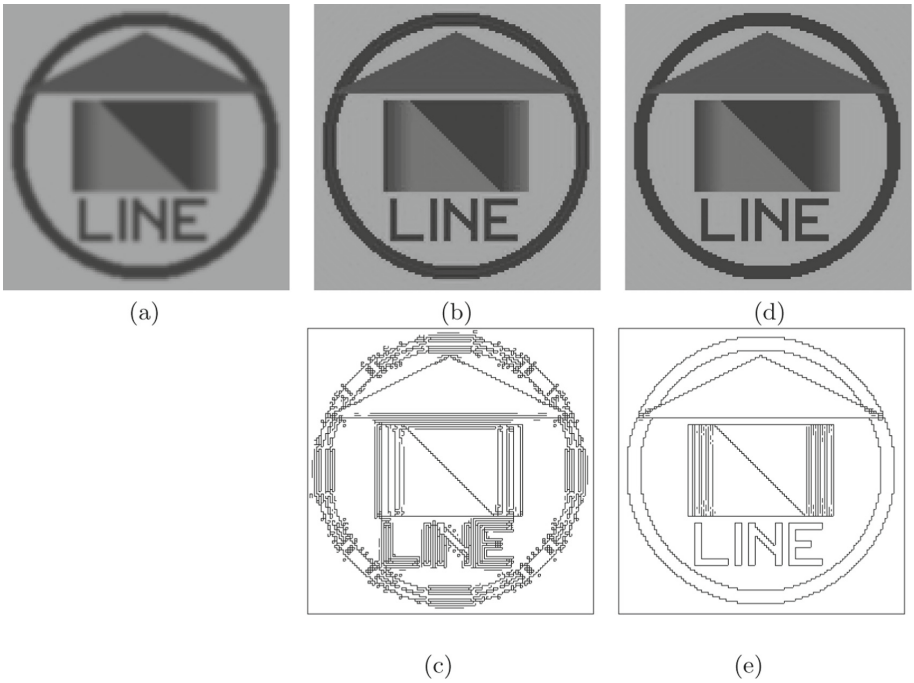

Fig. 5. In (a) the original blurred image; in (b) and (c) a reconstruction with $\varepsilon = 0$ and the corresponding line process plot; in (d) and (e), a reconstruction with $\varepsilon > 0$ and the corresponding line process plot.

To reduce the computational cost of the minimization of (Eq. 4), the *dual energy function* through the minimization of the primal energy function concerning the line process $\mathbf{w}$ is used. Namely, we get (see, e.g., [4,5])

$$E_d(\widetilde{\mathbf{l}}) = \inf_{\mathbf{w}} E(\widetilde{\mathbf{l}}, \mathbf{w}).$$

In general, the direct calculation of the dual energy function is difficult, so we consider the following good approximation of the dual energy function (see, e.g., [5]):

$$E_d(\widetilde{\mathbf{l}}) = \|A\widetilde{\mathbf{l}} - \mathbf{l}\|^2 + \sum_{c \in C_2} \psi(D_c^2\widetilde{\mathbf{l}}, D_{c-1}^2\widetilde{\mathbf{l}}),$$

where

$$\psi(t_1, t_2) = \begin{cases} \begin{cases} \lambda^2 t_1^2, & \text{if } |t_1| < s, \\ \theta, & \text{if } |t_1| \geq s, \end{cases} & \text{if } |t_2| < s, \\ \begin{cases} \lambda^2 t_1^2, & \text{if } |t_1| < \bar{s}, \\ \theta + \varepsilon, & \text{if } |t_1| \geq \bar{s}, \end{cases} & \text{if } |t_2| \geq s. \end{cases} \tag{5}$$

The quantity

$$s = \sqrt{\theta}/\lambda \tag{6}$$

is a *threshold* for creating a discontinuity, while $\bar{s} = \sqrt{\theta + \varepsilon}/\lambda$ is a *superthreshold* for creating a close parallel discontinuity. The function ψ in (Eq. 5) is plotted for particular values of λ, θ and $\varepsilon > 0$.

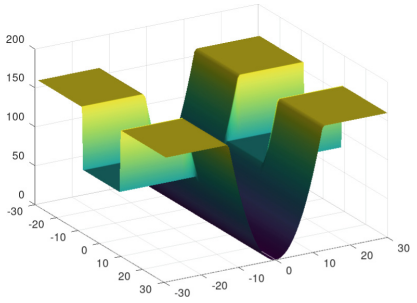

Fig. 6. Used stabilizers with $\lambda = 1$, $\theta = \varepsilon = 80$

The dual energy function E_d is not convex, and thus requires appropriate optimization strategies. A classical deterministic technique for minimizing the dual energy function is the GNC (*Graduated Non-Convexity*) algorithm (see, e.g., [2,5,7,10,14,17,18,22,23]). Algorithms for minimizing a non-convex function depend on the choice of the starting point; to perform a suitable choice of this point, the The GNC technique finds a finite family of approximating functions $\{E_d^{(p)}\}_p$, such that the first one is convex, and the last one is the original dual energy function. The GNC algorithm is defined as follows:

initialize $\widetilde{\mathbf{l}}$;
while $E_d^{(p)} \neq E_d$ do

- find the minimum of the function $E_d^{(p)}$ starting from the initial point $\widetilde{\mathbf{l}}$;
- $\widetilde{\mathbf{l}} = \arg\min E_d^{(p)}(\widetilde{\mathbf{l}})$;
- update the parameter p.

Chrominance Deblurring. Now we deal with reconstructing the chrominance component. The direct problem is formulated as follows:

$$\boldsymbol{\alpha} = A\,\widetilde{\boldsymbol{\alpha}} + \mathbf{n}_{\boldsymbol{\alpha}},\ \boldsymbol{\beta} = A\,\widetilde{\boldsymbol{\beta}} + \mathbf{n}_{\boldsymbol{\beta}},$$

where the vectors $\boldsymbol{a}$, $\widetilde{\boldsymbol{\alpha}}$, ($\boldsymbol{\beta}$, $\widetilde{\boldsymbol{\beta}}$), of dimension $n\,m$, are the observed chrominance α-component (β-component) and the ideal one in the lexicographic order, respectively. Note that we assume that the A matrix is the same as in the luminance step; experiments show that such a choice delivers satisfying reconstructions. The $n\,m$-dimensional vector $\mathbf{n}_{\boldsymbol{\alpha}}$ (resp. $\mathbf{n}_{\boldsymbol{\beta}}$) is the additive noise on the chrominance α-component (β-component), which is supposed to be white, Gaussian, with zero mean and a known variance σ^2.

We define the estimate of the solution as a minimizer of the following energy function:

$$E(\widetilde{\boldsymbol{\alpha}}, \boldsymbol{\beta}) = \|A\widetilde{\boldsymbol{\alpha}} - \boldsymbol{\alpha}\|^2 + \|A\widetilde{\boldsymbol{\beta}} - \boldsymbol{\beta}\|^2 + \sum_{c \in C_1} \lambda^2 (D_c^1 \widetilde{\boldsymbol{\alpha}})^2 + (D_c^1 \widetilde{\boldsymbol{\beta}})^2)(1 - \widetilde{w}_c). \quad (7)$$

where the first two terms of the right hand of (Eq. 7) are the faithfulness with data of the α- and the β-component of the chrominance, respectively, and the third addend is a smoothness term, in which λ^2 is the regularization parameter, which we assume to be the same as that used to reconstruct the luminance. Note that we use a finite difference operator of the first order, since we assume that chrominance is represented by a piecewise constant function. Moreover the line variables $\widetilde{w}_c$, with $c \in C_1$, are fixed by means of the estimated luminance $\widetilde{l}$, as follows:

$$\widetilde{w}_c = \begin{cases} 1 \text{ if } D_c^1 \widetilde{\mathbf{l}} \geq s, \\ \\ 0 \text{ otherwise,} \end{cases}$$

where s is as in (Eq. 6). Note that the energy function defined in (Eq. 7) is convex, and hence the minimization can be performed using a SOR-type algorithm.

4 Experimental Results

We present the application of the proposed algorithm to a set of faded images, to demonstrate the reconstruction capability and visually compare the results when different color spaces are used.

In Fig. 7 and Fig. 8 the observed and the corresponding reconstructed images are shown, using respectively the spaces QTLC-r_*^2 and QTLC-g_*^2. The parameters used in the defading phase in both cases are $l_0 = 100$, $c_l = 1.2$, $l_\alpha^+ = 0.4$, $c_\alpha^+ = 1.2$, $l_\alpha^- = 0.01$, $c_\alpha^- = 1.4$, $l_\beta^+ = 0.03$, $c_\beta^+ = 1.3$, $l_\beta^- = 0.01$, and $c_\beta^- = 1.5$; while the parameters used in the deblurring phase are $\lambda = 1$, $\theta = 10$, and $\epsilon = 10$. Moreover, we assume that the following blur mask blurs the observed data:

$$M = \begin{pmatrix} 5 & 10 & 5 \\ 10 & 20 & 10 \\ 5 & 10 & 5 \end{pmatrix}$$



(a) (b)

Fig. 7. (a): the observed image of dimension $n = 1160$; (b): the image reconstructed using the space QTLC-r_*^2.

Regarding the QTLC-r_*g_* space, we experimentally observed a higher degree of freedom in the choice of the parameter values for the defading process. Such behavior could be attributed to a superior uniformity of the space if compared to the previous two; for this reason, QTLC-r_*g_* should be the space of choice due to its more consistent capability of preserving color naturalness. In Fig. 9, (b) is reconstructed from (a), using the following defading parameters: $l_0 = 100$, $c_l = 1.1$, $l_\alpha^+ = 0.32$, $c_\alpha^+ = 1.6$, $l_\alpha^- = 0.005$, $c_\alpha^- = 3.8$, $l_\beta^+ = 0.08$, $c_\beta^+ = 1.5$, $l_\beta^- = 0.01$, and $c_\beta^- = 2$. The restoration capabilities of the three QTLC spaces and the LAB space are visually compared with the source image in Fig. 10. (b), (c), and (d) are obtained from (a) using respectively, the QTLC-r_*^2 (b), QTLC-g_*^2 (c), QTLC-$r_*\, g_*$ with the following common parameter values: $l_0 = 100$, $c_l = 1.1$, $l_\alpha^+ = 0.99$, $c_\alpha^+ = 1.1$, $l_\alpha^- = 0.005$, $c_\alpha^- = 2.8$, $l_\beta^+ = 0.08$, $c_\beta^+ = 1.5$, $l_\beta^- = 0.01$, $c_\beta^- = 1.5$; in (e) the CIE $L^*a^*b^*$ is employed, with $l_0 = 70$, $c_l = 1.1$, $l_{a^*}^+ = 50$, $c_{a^*}^+ = 1.3$, $l_{a^*}^- = -15$, $c_{a^*}^- = 1.3$, $l_{b^*}^+ = 10$, $c_{b^*}^+ = 1.3$, $l_{b^*}^- = -15$, $c_{b^*}^- = 1.3$. In both cases, the parameters taken to obtain Fig. 7 and Fig. 8 are used in the deblurring phase.



(a)



(b)

Fig. 8. (a): the observed image of dimension $n = 1166$; (b): the image reconstructed using the space QTLC-g_*^2.



(a)



(b)

Fig. 9. (a): the observed image of dimension $n = 1180$; (b): the image reconstructed using the space QTLC-$r_* g_*$.

In Fig. 11, details of the reconstructions obtained from the source in Fig. 10 are shown to highlight the differences between the QTLC spaces. (a) and (b) show a section of the bridge for the QTLC-r_*^2 and QTLC-$r_*\, g_*$ spaces; in the former, the colors tend to be over-saturated, while in the latter, they are more realistic. (c) and (d), instead, present a detail of the water in the canal for the QTLC-g_*^2 and QTLC-$r_*\, g_*$ spaces; in the first, the colors tend to be metallic, while in the QTLC-$r_*\, g_*$ reconstruction, the water hue is more natural.

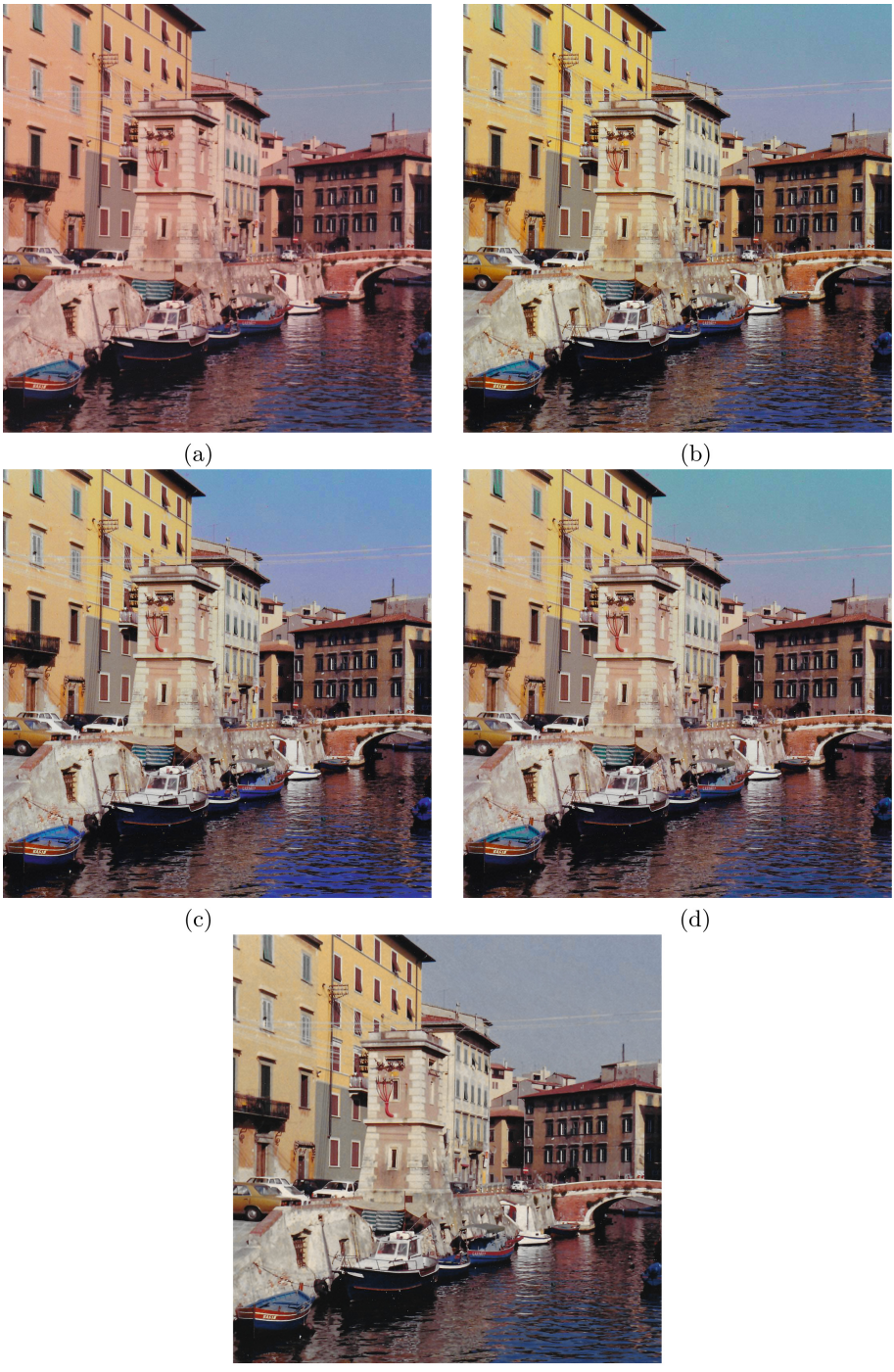

(a) (b) (c) (d) (e)

Fig. 10. (a): the observed image of dimension $n = 1077$; the image reconstructed using the QTLC-r_*^2 (b), QTLC-g_*^2 (c), QTLC-$r_*\, g_*$ (d), and CIE $L^*a^*b^*$ (e) spaces.

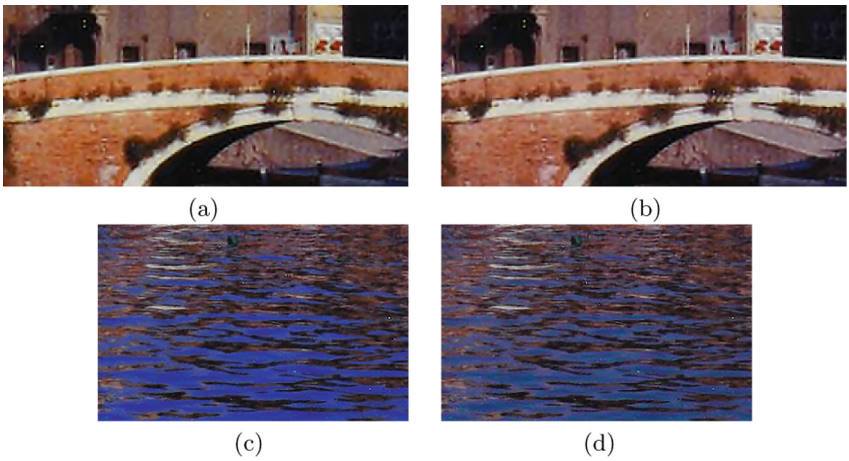

Fig. 11. A close-up of the bridge in Fig. 10, from the image reconstructed with QTLC-r_*^2 (a) and QTLC-$r_*\, g_*$(b); A close-up of the water section in Fig. 10, from the image reconstructed with QTLC-g_*^2 (c) and QTLC-$r_*\, g_*$(d)

Conclusions

In this work, we defined three new color spaces obtained by means of a quadratic transform from the RGB space. To test the uniformity of such spaces, we employed them to deal with the image defading problem, using a novel two-step technique: first, we defined a fast heuristic to restore the correct color saturation; then, we proposed a regularization technique to deblur the analyzed image. We experimentally observed that presumably thanks to its higher uniformity, the QTLC-r_*g_* space widens the range of parameter values that produce natural-looking images in the reconstruction and should thus be preferred to the QTLC-r_*^2 and QTLC-g_*^2 spaces.

References

1. Ahmed, A.M.T.: Color restoration techniques for faded colors of old photos, printings, and paintings. In: Proceedings of 2009 IEEE International Conference on Electro/Information Technology, pp. 151–156 (2009)
2. Boccuto, A., Gerace, I.: Image reconstruction with a non-parallelism constraint. In: Proceedings of the International Workshop on Computational Intelligence for Multimedia Understanding, Reggio Calabria, Italy, 27–28 October 2016, pp. 1–5. IEEE Conference Publications (2016)
3. Boccuto, A., Gerace, I., Giorgetti, V., Rinaldi, M.: A fast algorithm for the demosaicing problem concerning the Bayer pattern. Open Signal Process. J. **6**, 1–14 (2019)

4. Boccuto, A., Gerace, I., Martinelli, F.: Half-quadratic image restoration with a non-parallelism constraint. J. Math. Imaging Vision **59**(2), 270–295 (2017)
5. Boccuto, A., Gerace, I., Pucci, P.: Convex approximation technique for interacting line elements deblurring: A new approach. J. Math. Imag. Vis. **44**(2), 168–184 (2012)
6. Bruni, V., Ramponi, G., Restrepo, A., Vitulano, D.: Context-based defading of archive photographs. EURASIP J. Image Video Process. **2009** 986183 (2009)
7. Cricco, F., De Santi, G., Gerace, I.: A deterministic algorithm for deblurring considering higher order smoothness constraints. In: Proceedings of the 2003 International Workshop on Spectral Methods and Multirate Signal Processing (SMMSP) 2004, Vienna, pp. 325–332 (2004)
8. Demoment, G.: Image reconstruction and restoration: Overview of common estimation structures and problems. IEEE Trans. Acoust. Speech Signal Process. **37**, 2024–2036 (1989)
9. Ebner, F., Fairchild, M.: Development and testing of a color space with improved hue uniformity. In: Proceedings of The Sixth Color Imaging Conference: Color Science, Systems, and Applications, Scottsdale, Arizona, USA, pp. 8–13 (1998)
10. Evangelopoulos, X., Brockmeier, A.J., Mu, T., Goulermas, J.Y.: A graduated non-convexity relaxation for large-scale seriation. In: Proceedings of the 2017 SIAM International Conference on Data Mining, Houston, Texas, pp. 462–470 (2017)
11. Fairchild, M.D.: Color and Image Appearance Models. Color Appearance Models. John Wiley and Sons (2005)
12. Gerace, I., Martinelli, F., Pucci, P.: A deterministic algorithm for optical flow estimation. Commun. Appl. Indust. Math. **1**(2), 249–268 (2010)
13. Gunturk, B.K., Altunbasak, Y., Mersereau, R.M.: Color plane interpolation using alternating projections. IEEE Trans. Image Process. **11**(9), 997–1013 (2002)
14. Hazan, E., Levy, K.Y., Shalev-Shwartz, S.: On graduated optimization for stochastic non-convex problems. In: Proceedings of the 33rd International Conference on Machine Learning, New York, 2016. JMLR: W& CP, vol. 48, pp. 1–9 (2016)
15. Kyung, W.J., Kim, K.M., Kim, D.C., Ha, Y.H.: Color correction for a faded image using classification in LCybCrg color space. In: 2011 IEEE International Conference on Consumer Electronics-Berlin (ICCE-Berlin), pp. 189–193 (2011)
16. Liu, W., Ribeiro, E.: A survey on image-based continuum-body motion estimation. Image Vis. Comput. **29**(8), 509–523 (2011)
17. Liu, Z.-Y., Qiao, H.: GNCCP-graduated nonconvexity and concavity procedure. IEEE Trans. Pattern Anal. Mach. Intell. **36**(6), 1258–1267 (2014)
18. Liu, Z.-Y., Qiao, H., Su, J.-H.: MAP inference with MRF by graduated non-convexity and concavity procedure. In: Loo, C.K., Yap, K.S., Wong, K.W., Teoh, A., Huang, K. (eds.) ICONIP 2014. LNCS, vol. 8835, pp. 404–412. Springer, Cham (2014). https://doi.org/10.1007/978-3-319-12640-1_49
19. Nikitenko, D., Wirth, M., Trudel, K.: Applicability of white-balancing algorithms to restoring faded colour slides: An empirical evaluation. J. Multim. **3**(5), 9–18 (2008)
20. Restrepo, A., Ramponi, G.: Filtering and luminance correction for aged photographs. In: Image Processing: Algorithms and Systems VI, Proceedings of SPIE, San Jose, Calif, vol. 6812, pp. 26–31 (2008)

21. Panetta, K.A., Wharton, E.J., Agaian, S.S.: Human visual system-based image enhancement and logarithmic contrast measure. IEEE Trans. Syst. Man Cybernet. **38**(1), 174–188 (2008)
22. Smith, T., Egeland, O.: Dynamical pose estimation with graduated non-convexity for outlier robustness. Model. Identificat. Control **43**(2), 79–89 (2022)
23. Yang, H., Antonante, P., Tzoumas, V., Carlone, L.: Graduated non-convexity for robust spatial perception: From non-minimal solvers to global outlier rejection. IEEE Robot. Automat. Lett. **5**(2), 1127–1134 (2020)